Synthetic Aperture Focusing Technique for Correction of Poorly-Focused Ultrasonic Pressure Tube Inspection Data

Huan Zhao, Anthony Gachagan, Gordon Dobie, Christopher Wallace, Graeme West
Electronic and Electrical Engineering, University of Strathclyde
Glasgow, G1 1XW, United Kingdom
huan.zhao@strath.ac.uk

Abstract

Defect size measurement of ultrasonic pressure tube inspection within the CANDU (CANada Deuterium Uranium) reactor has challenges when the transducer is poorly-focused with respect to the tube surface. Environmental effects, such as diametrical creep and sagging over time can lead to displacement of the tube surface from the optimal inspection position. In order to improve the accuracy of defect sizing, a Synthetic Aperture Focusing Technique (SAFT) method based on single element focused transducer inspection is proposed. In SAFT processing, the transducer focal point operates as a virtual source to transmit ultrasound with a corresponding beam angle relating to the transducer aperture and focal length. To correct for the image distortion caused by poor focusing in the region beyond the transducer focal point, every pixel value of the B-scan image is calculated using the delay-and-sum of echo signals collected at multiple positions on the synthetic aperture, while the synthetic aperture length is determined by the beam angle of the virtual source. Application of the SAFT approach significantly enhances image resolution through which more accurate feature size measurements can be determined, with the accuracy of a -6dB measured surface defect width improved by 50% compared to the original B-scan image when the surface is located more than 1.5mm beyond the focal point.

1. Introduction

Pressure tubes are used in a CANDU nuclear reactor to locate the fuel bundles and to support the coolant passing through to remove the heat from the fuel [1]. This zirconium alloy part plays the key role in maintaining the reliability of the reactor performance. Therefore, regular inspection of the pressure tubes is particularly important to ensure their operating condition is qualified. The pressure tubes are about 6.3 m long, 104 mm inner diameter and 4.3 mm thickness. During the operation, they are exposed to a pressure of approximately 10 MPa and temperatures ranging from 250℃ to 310℃ [2]. Due to the harsh environment of high temperature, pressure and neutron flux, the tube dimensions change during their service such as axial elongation, diametric expansion, sagging and wall thinning. Consequently, the inspection of the pressure tubes faces challenges to overcome the difficulties brought by tube dimensional changes.

A focused ultrasonic technique is used for the pressure tube inspection. This presents challenges since the transducer is not always aligned as expected, due to the tube dimensional changes. The focused transducer is designed to be immersed in heavy water and to perform a helical scan inside of the tube and focus on the tube inner surface. However, the poorly-focused transducer can produce to a defocused B-scan

image which leads to the oversizing of defects. This is worse in the middle of the tube where sagging causes the biggest difference from the ideal position. Defects beyond a specific dimensional threshold are then sized in more detail by a time and cost consuming replica process [3]. Defect width is one of the main factors for making a decision on whether to execute the replica process [4]. More accurate ultrasonic sizing would reduce the need for replicas. In order to improve the measurement accuracy, Synthetic Aperture Focusing Technique (SAFT) is proposed in this paper for correction of the poorly-focused ultrasonic pressure tube inspection data.

SAFT was first applied in the field of radar and it has been utilised for over 30 years in ultrasonic Non-Destructive Testing (NDT) to improve the detection performance in terms of horizontal resolution, defect sizing and improved Signal Noise Ratio (SNR) [5] [6][7][8]. It has been applied to both pulse echo and phased array modes of operation [9][10][11]. SAFT has been researched in anisotropic and strongly attenuating material. Spies analysed the methods for modelling of ultrasonic NDT of anisotropic media that was simulated by a Gaussian beam and a point source superposition technique [12]. Jager and Spies conducted experiments on carbon-fiber reinforced composites containing Side-Drilled Holes (SDH) and Flat-Bottom Holes (FBH) to validate the algorithm [13]. Moreover, Spies and Rieder used SAFT in the determination of the Probability of Detection (POD) in strongly attenuating material [14]. More research on SAFT has been implemented using data collected from phased array transducers because the small size of single transducer element meets the beam divergence characteristic criteria of SAFT. Boehm et al. modelled phased array inspection with different angles of incidence to collect data for SAFT analysis [9] and performed experiments on test samples for validation. They concluded that compared to SAFT using a conventional transducer, the key advantage was an improved SNR, while the disadvantage was the increased amount of raw data. Researchers also made comparisons between SAFT, Full Matrix Capture (FMC) / Total Focusing Method (TFM) and Time-of-Flight Diffraction (TOFD). Holmes et al. used a typical synthetic aperture sonar approach, Range-Doppler algorithm, to process pulse-echo data which could reduce the image process time compared to TFM [15]. Compared with TOFD, SAFT is better in the capabilities of detection and sizing due to its superior spatial resolution [16]. Applications in concrete inspection also show SAFT's advantages in ultrasonic imaging processing [17][18]. In addition, SAFT in the frequency domain has been investigated, including the main aspects of Phase Shift Migration (PSM) algorithm [19][20] and ω-k algorithm [21][22].

In recent years, the SAFT algorithm with a virtual source has been researched by many scholars to take advantage of the focal point of the transducer either using a focused transducer or a phased array transducer working with a focused delay law. Frazier and O'Brien proposed a virtual source synthetic aperture technique for a focused transducer to test wire and cyst objects with different weighting functions [23]. They proved that by using the SAFT method a better resolution and increased image SNR could be achieved even when the test object was 3, 5 and 7 mm beyond the focal point. Another weighting method was presented by Li et al. for virtual source SAFT, which considered ultrasonic energy in the frequency domain [24]. Scharrer et al. presented a new method for data acquisition which executed a scan at each position to manipulate the incidence angle on the surface of the test object [25]. This SAFT processing approach had good

performance in identifying inner structural edges. The application of virtual source SAFT in phased array transducer applications was introduced by Bae and Jeong [26]. They utilized the virtual source for both forward and back directions and showed the result of the SAFT algorithm for medical applications. Furthermore, a virtual source SAFT method in frequency domain was presented by Wu et al. for improving the lateral resolution of the image [27].

This paper investigates the capability of the SAFT algorithm to improve the accuracy of defect width measurements and analyses the effects of transducer focal length value in terms of algorithm performance. The paper is organized as follows: the methodology of SAFT is described in Section 2; the SAFT process of industrial data and the effects of different focal length values are introduced in Section 3; Section 4 demonstrates the processing results with different focal lengths and the corresponding -6 dB defect contour; and the discussion and conclusion are presented in Section 5.

2. Methodology

2.1 Problem definition

In the inspection of pressure tubes within a CANDU reactor, ultrasonic single element focused transducers are employed to collect normal beam pulse-echo data (10 MHz and 20 MHz transducers) and full-skip shear wave pitch-catch data (10 MHz transducers) [28]. Currently, only the 10 MHz transducers are applied for the defect width measurement by using either the 'visual' sizing or the amplitude drop method. These approaches have limited accuracy due to human error and 'jitter' interference, respectively [4]. The 20 MHz transducer provides higher frequency inspection data and an intuitive B-scan image for defect detection and sizing. It therefore has a huge potential for accurate defect width measurement. However, the in-service tube dimensional changes led to the transducer being poorly-focused with respect to the tube inner surface which causes poor inspection results. Thus, a SAFT algorithm is proposed to overcome this system focus challenge to improve the inspection accuracy.

2.2 Basic SAFT theory

SAFT theory extends the aperture of a physical source by processing multiple sequential echo signals. The basic concept of SAFT involves manipulating a single element transducer to collect pulse-echo signals. Importantly, each point in the ROI (Region of Interest) can be inspected at multiple transducer positions due to the divergence of ultrasonic beam angle.

The usual implementation method utilises delay-and-sum (DAS) in the time domain to summarize all the signal values on the aperture to one pixel value [29]. As shown in Figure 1 (a), a transducer is moved step by step to collect echo information from point P. The echoes from P can be received at many transducer positions and relate to different time delays in the B-scan image, as presented in Figure 1 (b). Summing all the pixel values on the aperture to produce a pixel value at P is called the DAS method and the SAFT B-scan image executes the process for all the image pixels.

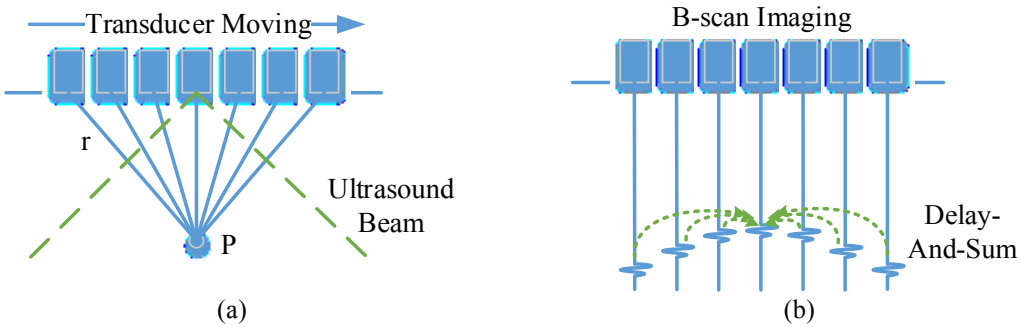

Figure 1. SAFT theory, (a) inspection data collection; (b) delay-and-sum in B-scan image

The calculation of new pixel value p can be determined using Equation 1, where $e_i(t)$ is the echo signal acquired at position i. k is the length of the aperture (also considered as the number of transducer positions within the aperture). r_i is the distance from the transducer to the target point at position i and c is the longitudinal wave velocity in the medium.

$$p = \sum_{i=1}^{k} e_i\left(\frac{2r_i}{c}\right) \tag{1}$$

2.3 SAFT theory for focused transducer

When a focused transducer is employed in the SAFT algorithm, the wave propagation path for delayed time calculation is different from that of an unfocused transducer. In terms of a focused transducer, the ultrasound beam beyond the focal point is applied for synthetic aperture processing [23]. As Figure 2 (a) shows, the wave propagation paths to P from two transducer positions are ACP and BDP respectively. The time difference can be calculated from paths CP and DP, since the focused transducer has same propagation distance from the transducer surface to the focal point. However, for an unfocused transducer, the wave propagation path is determined from the transducer centre point to P, which are shown as A'C'P' and B'D'P' in Figure 2 (b). The difference between paths ACP and A'C'P' is obvious from Figure 2 and therefore the DAS approach needs to be adjusted to accommodate the focal point plane for focused transducer.

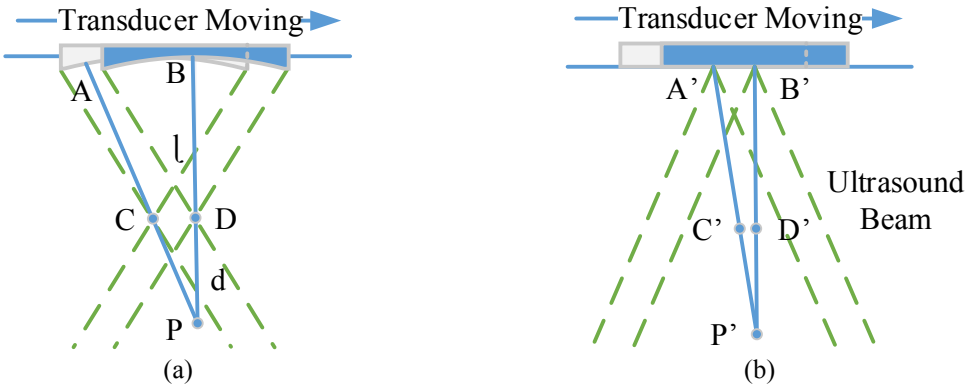

Figure 2. Wave propagation path, (a) focused transducer; (b) unfocused transducer

The calculation of new pixel value p_f can be described in Equation 2, where l is the focal length of the transducer and d_i is the distance from the focal point at transducer position i to the target point.

$$p_f = \sum_{i=1}^{k} e_i\left(\frac{2(l + d_i)}{c}\right) \tag{2}$$

2.4 Focal length and synthetic aperture

When the transducer focal length changes, it results in time differences between data collected at neighbouring positions. Since the transducer used for our industrial application is reported to have a Focal Length (FL) of 10.4 mm, a selection of FL equal to 10.4 mm, 12 mm and 13.5 mm is used in this work, as shown in Figure 3, in which the red line indicates the synthetic aperture. When applying SAFT to the same point of a B-scan image, a longer focal length value produces a shorter length and higher curvature aperture, as shown in Figure 3. Here, shorter means less sample points on the moving axis. In Section 3.4, the theoretically calculated synthetic apertures for different focal length values are drawn on the B-scans to facilitate visual comparison.

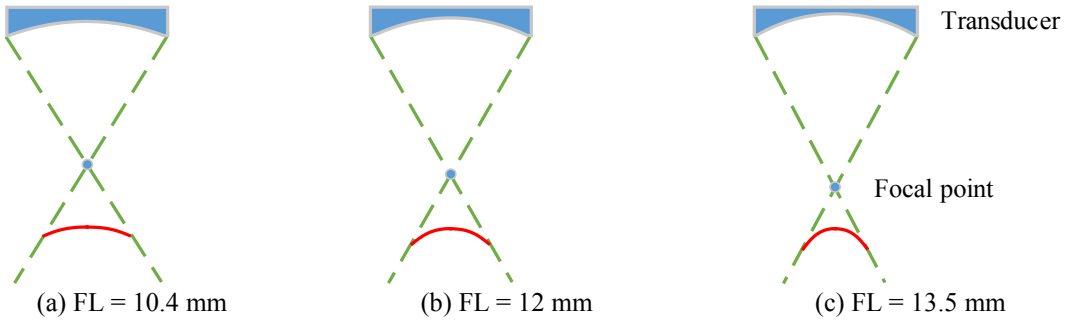

Figure 3. Relationship between focal length and synthetic aperture (red line), (a) FL = 10.4 mm; (b) FL = 12 mm; (c) FL = 13.5mm

3. SAFT processing of industrial data

3.1 Data acquisition

In this industrial inspection, a sensor head named CIGAR (Channel Inspection and Gauging Apparatus for Reactors) containing ultrasonic transducers is immersed in heavy water to execute a helical scan inside of the pressure tubes. The 20 MHz transducer is working in normal beam pulse-echo mode to acquire A-scan signals and then the data is utilized to produce a B-scan image, which will be further processed using SAFT.

3.2 SAFT processing parameters

The 20 MHz focused transducer has a diameter of 6.3 mm and a focus at 10.4 mm. Different virtual focal lengths are considered in the following SAFT processing to show the effects of focal length to the algorithm performance, which are 10.4 mm, 12 mm and 13.5 mm. Table 1 lists all the key parameters for SAFT processing.

Table 1. Parameters for SAFT processing

Parameter	Value
Transducer frequency	20 MHz
Transducer diameter	6.3 mm
Transducer focal length	10.4/12/13.5 mm
Sample frequency	100 MHz
Cable signal delay	700 ns
Wave velocity in heavy water	1420 m/s

3.3 Flowchart

The SAFT algorithm is executed in MATLAB R2016b (The MathWorks, Inc.) and the flowchart is presented in Figure 4. Since the transducer is performing a helical scan inside of the tube to collect data, the tube surface on the B-scan image is not straight. Therefore, prior to applying the SAFT algorithm, the tube surface is straightened by using the Random Sample Consensus (RANSAC) method [30].

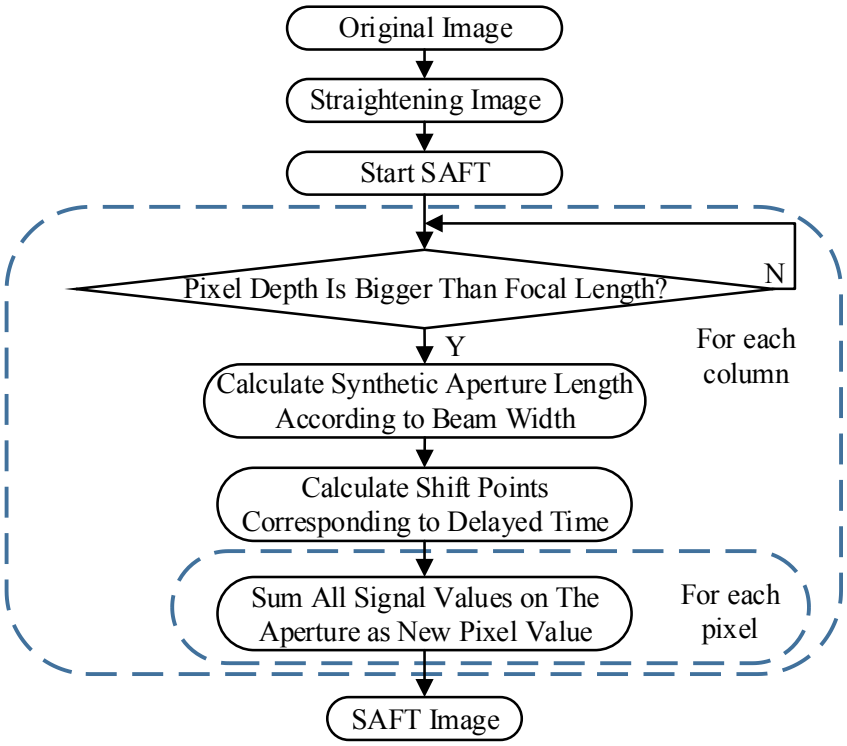

Figure 4. Flowchart of SAFT algorithm on inspection data from a focused transducer

In the inspection system's display mode, the horizontal axis of the B-scan image indicates time and the vertical axis indicates the rotational degree. Therefore, the B-scan data is a 2-D matrix with each column showing the echo signal at a specific time and each row showing signal received at a specific position. The steps of SAFT processing are listed as follows:

- For each column, evaluate if the pixel depth is bigger than focal length. The pixel depth is the distance between the target pixel and the transducer surface.
- If yes, calculate the length of the synthetic aperture according to the transducer beam width.

- Calculate the shift points within the synthetic aperture corresponding to the delayed time. The shift points are all the pixels on the aperture with respect to the central pixel (it has a distance d_0 to the focal point) that can be calculated by $\Delta t_i * f = \left[\frac{2(l+d_i)}{c} - \frac{2(l+d_0)}{c}\right] * f$ for each transducer position i (f is the sample frequency).
- For each pixel, sum all the signal values on the aperture and record as the new pixel value.

After all the pixels on the B-scan image have been replaced by the new pixel values, a SAFT B-scan image is obtained.

3.4 Effects of Using Different Focal Length Values

Figure 5 presents a CIGAR data example of calculated apertures overlaid on a B-scan image with the 3 different focal length values. In this B-scan example, the potential defect is detected and the corresponding echo signals can be seen as curved lines beneath the tube surface in the grey-scale image. The calculated transducer apertures are indicated by the red dotted lines. When using 10.4 mm as focal length value for the aperture calculation, the aperture length is a reasonably close match to the length of the echo signal, but the curvature is smaller. While the 12 mm focal length value produces an aperture curvature very well matched to the echo signal, but with a shorter length. Finally, for the case of the focal length equal to 13.5 mm, the aperture curvature is larger than the practical one and the length is the shortest. In Figure 5(c), since the aperture length is too short to illustrate the curvature, an extension of aperture is indicated by the green dotted line.

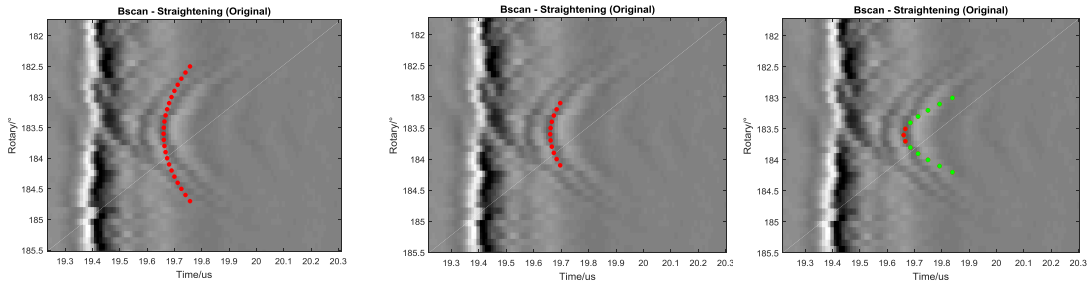

(a) FL = 10.4 mm (b) FL = 12 mm (c) FL = 13.5 mm

Figure 5. Calculated aperture on B-scan image by different focal length values, (a) FL = 10.4 mm; (b) FL = 12 mm; (c) FL = 13.5 mm

4. Result Analysis of Different Focal Length Values

Figure 6 presents SAFT processing results with different focal length values and the corresponding -6 dB defect contour. The propagation time for ultrasound reaching the tube surface is approximately 19.4 us. The left column shows the B-scan images and the right column displays the -6 dB defect contour.

In this CIGAR data example, an obvious ‘over-correction’ phenomenon can be found in SAFT B-scan by applying focal length value of 10.4 mm (Figure 6 (b)), but importantly the first reflected echo from the defect is no longer visible in the -6 dB defect contour. This ‘over-correction’ phenomenon indicates the change of the defect’s curved direction.

It is caused by the accumulation of additional echo signals not belonging to the target. In other words, the theoretical synthetic aperture and the practical one should be matched to take the advantage of the SAFT algorithm. Then, the accumulation of the pixel values on the aperture is considered to be accurate or 'true' focusing. Likewise, for the case of utilizing a focal length value of 13.5 mm, because the theoretical synthetic aperture and the practical one are not matched, as shown in Figure 5 (c), a poor focusing result is produced, as illustrated in Figure 6 (d). The focal length value of 12 mm demonstrates a well matched synthetic aperture, as shown in Figure 5 (b), and this produces the well-focussed SAFT B-scan image presented in Figure 6 (c), which results in a defect width measurement result of 0.3 mm. Comparing this to the 0.8 mm result verified by an analyst, an improvement of 50% for the measurement is achieved.

5. Synthetic Aperture Length

When the tube surface and transducer focal point have a larger separation, the synthetic aperture is larger and more apparent in an image. Consequently, when applying SAFT on such B-scan images, more directly relevant information can be utilized to get better correction. Figure 6 (a), (c) and Figure 7 show inspection data examples of the defects situated at different positions along the tube, where the B-scan images are listed on the left-hand side and the -6 dB defect contours are shown on the right-hand side. Since the tube centre is more susceptible to sagging, the tube surface is farthest from the transducer focal point (Example 1), while Example 2 presents the inspection at one quarter of the tube length and Example 3 presents the result at the end of the tube. The respective times to reach the tube surface are 19.4 us, 18.95 us and 17.7 us. In terms of the 20 MHz transducer with a focal length of 12 mm, the time to reach the tube surface should be approximately 16.9 us for a well-focused inspection.

In Figure 6 (c), when the tube surface is the furthest from the focal point, the SAFT image has the best resolution compared to the original image, which can be found in the defect -6 dB contour. The defect width has a much smaller size on SAFT B-scan than on the original B-scan which indicates a better focusing effect. In terms of the tube surface being closer to the focal point (Figure 7 (a)), the SAFT image has a good degree resolution comparing to the original image, but is not that well-focused as discussed for Example 1. Therefore, a smaller defect width can be found on the SAFT B-scan but this is not significantly different from the original size. Finally, when the tube surface is the closest to the focal point, the SAFT image has the similar degree resolution comparing to the original image with tiny difference between the defect widths, where the defects are indicated by red dashed ovals (Figure 7 (b)).

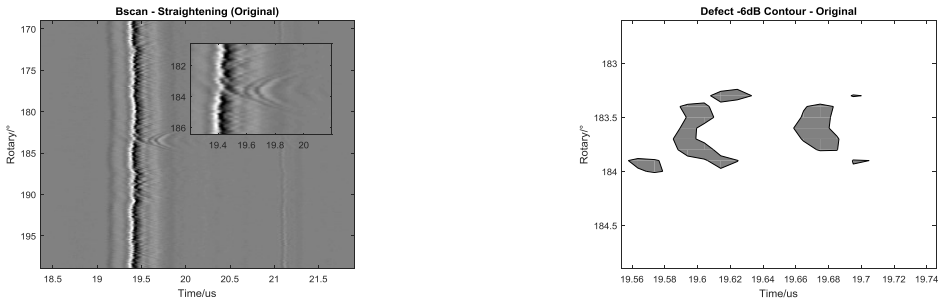

(a) Original B-scan and -6 dB contour shows typical 'poorly focused frown'

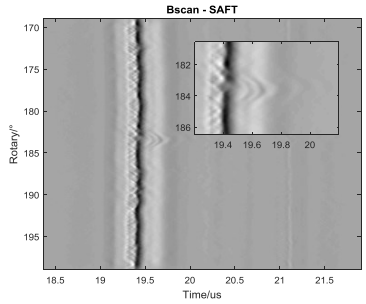

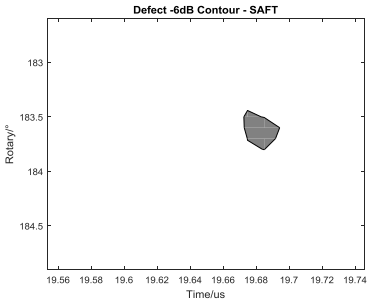

(b) SAFT B-scan (FL = 10.4 mm) and -6 dB contour shows 'over-correction'

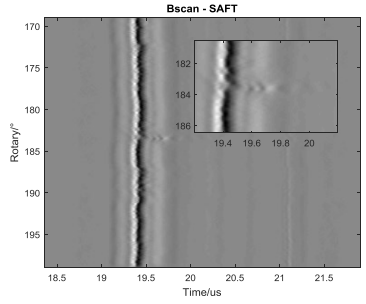

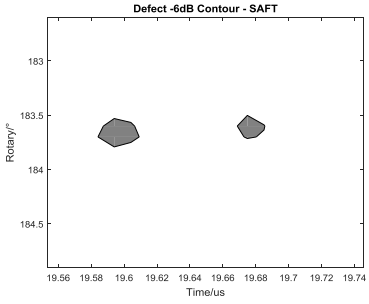

(c) SAFT B-scan (FL = 12 mm) and -6 dB contour shows good correction

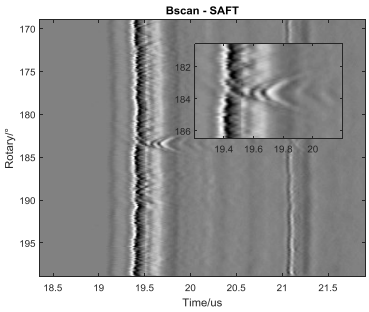

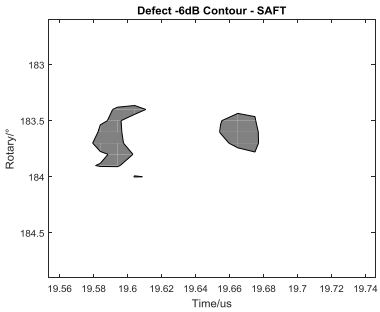

(d) SAFT B-scan (FL = 13.5 mm) and -6 dB contour shows poor correction

Figure 6. CIGAR data Example 1 SAFT processing result and corresponding -6 dB defect contour, (a) Original data; (b) SAFT (FL = 10.4 mm); (c) SAFT (FL = 12 mm); (d) SAFT (FL = 13.5 mm)

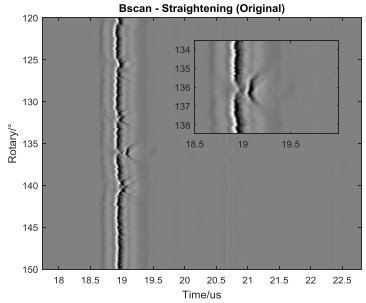

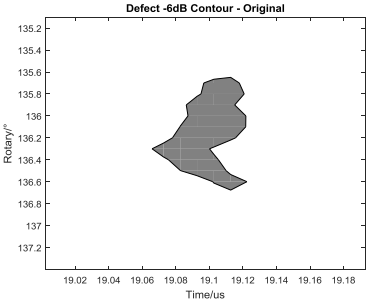

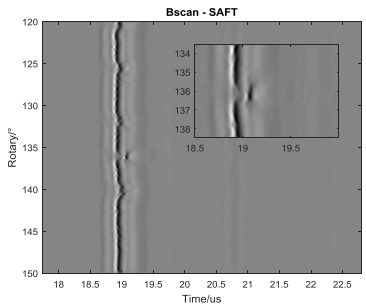

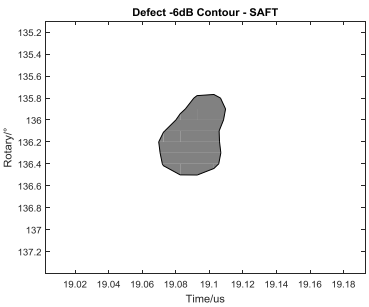

(a) Example 2: one quarter of the tube

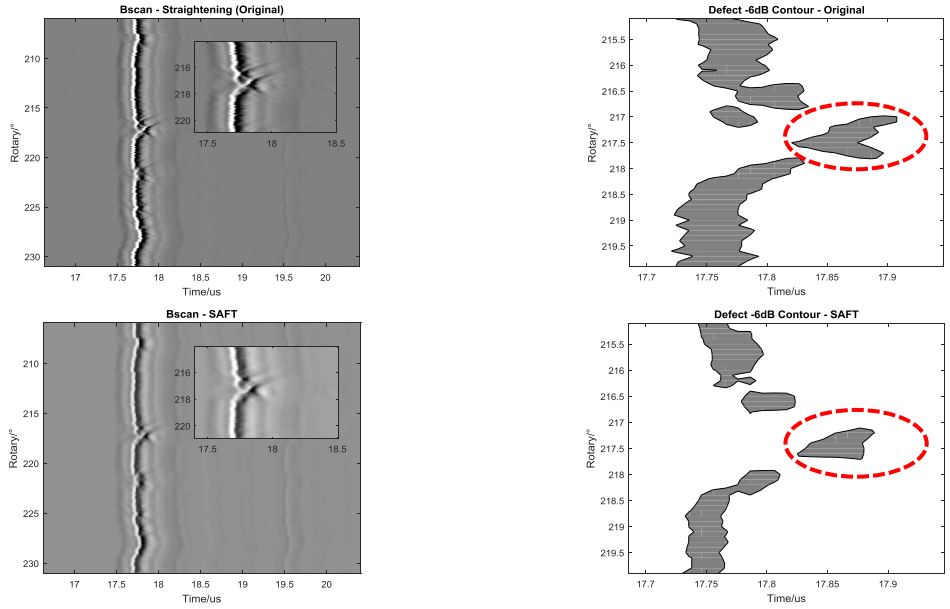

(b) Example 3: end of the tube

Figure 7. Original B-scan and defect -6 dB contour comparing to SAFT results (a) Example 2: one quarter of the tube; (b) Example 3: end of the tube

The results and errors of the defect width measured using the -6 dB method can be found in Table 2. The results demonstrate the defect width measurement on SAFT image has better focusing compared to the original image data, and the farthest distance (Example 1) separated from the tube surface brings about the best focusing result. Hence, there is a confidence that SAFT algorithm will contribute positively for the correction of poorly-focused inspection, especially for ageing pressure tubes.

Table 2. Defect width -6dB contour comparison – rotation degree axis

Example No.	Original Image (°)	SAFT Image (°)	|Δ| (°)
1	0.8	0.3	0.5
2	1.1	0.8	0.3
3	0.8	0.6	0.2

6. Conclusion

In this paper, SAFT processing of poorly-focused B-scan images from a CANDU pressure tube inspection is presented and the effect of different values of transducer focal length on SAFT processing is analysed. The SAFT algorithm for a focused transducer scenario is different from one for unfocused transducer, where the calculation of time difference between the neighbouring positions is different. Importantly, the transducer's focal length is a significant parameter for the SAFT processing, which determines if the calculated synthetic aperture is matched with the practical defect echo curve on B-scan image. A mismatched aperture could cause an 'over-correction' phenomenon in the SAFT processing result.

SAFT processing can improve the defect width measurement with a matched synthetic aperture. It increases resolution without any modification or extension to the CANDU inspection. Therefore, it provides a competitive solution for higher resolution defect

width measurement and has potential to bring about better correction for ageing tubes with more serious sag issues. Future work will characterise the algorithm on a wider range of defects and determine methods to automatically identify the focal point error.

Acknowledgements

The authors would like to thank the studentship sponsored by Duncan Hawthorne Scholarship for funding of Huan Zhao's PhD.

References

[1] IAEA - International Atomic Energy Agency, "Assessment and management of ageing of major nuclear power plant components important to safety: CANDU pressure tubes," 1998.

[2] A. C. Wallace, S. Xu, N. P. Singh, and L. Gutkin, "Inspection Specification for CANDU Fuel Channels," 2008.

[3] M. Trelinski, "Pressure tube flaws and artifacts observed in CANDU fuel channels ; detection , sizing and characterization issues," in *IV Conferencia Panamericana de END*, 2007.

[4] Candu Energy Inc., "Operating Procedure CIGAR Analysis- PT Inspection Data Analysis - Analysis of Ultrasonic Indications Engineering and Technical Delivery," 2014.

[5] J. A. Johnson and B. A. Barna, "The Effects of Surface Mapping Corrections with Synthetic-Aperture Focusing Techniques on Ultrasonic Imaging," *IEEE Trans. Sonics Ultrason.*, vol. 30, no. 5, pp. 283–294, 1983.

[6] S. R. Doctor, T. E. Hall, and L. D. Reid, "SAFT - the evolution of a signal processing technology for ultrasonic testing," *NDT Int.*, vol. 19, no. 3, pp. 163–167, 1986.

[7] V. Schmitz, S. Chakhlov, and W. Müller, "Experiences with synthetic aperture focusing technique in the field," *Ultrasonics*, vol. 38, no. 1, pp. 731–738, 2000.

[8] G. Dobie, S. Gareth Pierce, and G. Hayward, "The feasibility of synthetic aperture guided wave imaging to a mobile sensor platform," *NDT E Int.*, vol. 58, pp. 10–17, 2013.

[9] R. Boehm, D. Brackrock, J. Kitze, G. Brekow, and M. Kreutzbruck, "The SAFT Approach for Advanced Crack Analysis," in *Proceedings of the National Seminar and Exhibition on Non-Destructive Evaluation*, 2009, pp. 315–318.

[10] H. Zhao, "Ultrasonic Automatic Testing System for Large Thickness Welding," Shenzhen University, 2012.

[11] I. Bolotina *et al.*, "Ultrasonic arrays for quantitative nondestructive testing an engineering approach," *Russ. J. Nondestruct. Test.*, vol. 49, no. 3, pp. 145–158, 2013.

[12] M. Spies, "Analytical methods for modeling of ultrasonic nondestructive testing of anisotropic media," *Ultrasonics*, vol. 42, no. 1–9, pp. 213–219, 2004.

[13] M. Spies and W. Jager, "Synthetic aperture focusing for defect reconstruction in anisotropic media," *Ultrasonics*, vol. 41, no. 2, pp. 125–131, 2003.

[14] M. Spies and H. Rieder, "Synthetic aperture focusing of ultrasonic inspection data to enhance the probability of detection of defects in strongly attenuating materials," *NDT E Int.*, vol. 43, no. 5, pp. 425–431, 2010.

[15] C. Holmes, B. W. Drinkwater, and P. D. Wilcox, “Advanced post-processing for scanned ultrasonic arrays: Application to defect detection and classification in non-destructive evaluation,” *Ultrasonics*, vol. 48, no. 6–7, pp. 636–642, 2008.
[16] J. Prager, J. Kitze, C. Acheroy, D. Brackrock, G. Brekow, and M. Kreutzbruck, “SAFT and TOFD - A comparative study of two defect sizing techniques on a reactor pressure vessel mock-up,” *J. Nondestruct. Eval.*, vol. 32, no. 1, pp. 1–13, 2013.
[17] M. Schickert, M. Krause, and W. Müller, “Ultrasonic Imaging of Concrete Elements Using Reconstruction by Synthetic Aperture Focusing Technique,” *J. Mater. Civ. Eng.*, vol. 15, no. 3, pp. 235–246, 2003.
[18] K. Hoegh and L. Khazanovich, “Extended synthetic aperture focusing technique for ultrasonic imaging of concrete,” *NDT E Int.*, vol. 74, pp. 33–42, 2015.
[19] T. Olofsson, “Phase shift migration for imaging layered objects and objects immersed in water,” *IEEE Trans. Ultrason. Ferroelectr. Freq. Control*, vol. 57, no. 11, pp. 2522–2530, 2010.
[20] M. H. Skjelvareid, Y. Birkelund, and Y. Larsen, “Internal pipeline inspection using virtual source synthetic aperture ultrasound imaging,” *NDT E Int.*, vol. 54, pp. 151–158, 2013.
[21] T. Stepinski, “An Implementation of Synthetic Aperture Technique in Frequency Domain,” *IEEE Trans. UFFC*, vol. 54 (7), no. 7, pp. 1399–1408, 2007.
[22] M. H. Skjelvareid, T. Olofsson, Y. Birkelund, and Y. Larsen, “Synthetic aperture focusing of ultrasonic data from multilayered media using an omega-K algorithm,” *IEEE Trans. Ultrason. Ferroelectr. Freq. Control*, vol. 58, no. 5, pp. 1037–1048, 2011.
[23] C. H. Frazier and W. D. O’Brien, “Synthetic aperture techniques with a virtual source element,” *IEEE Trans. Ultrason. Ferroelectr. Freq. Control*, vol. 45, no. 1, pp. 196–207, 1998.
[24] M. Li, W. Guan, and P. Li, “Improved Synthetic Aperture Focusing Technique with Applications in High-Frequency Ultrasound Imaging,” *Engineering*, vol. 51, no. 1, pp. 63–70, 2004.
[25] T. Scharrer, M. Schrapp, S. J. Rupitsch, A. Sutor, and R. Lerch, “Ultrasonic imaging of complex specimens by processing multiple incident angles in full-angle synthetic aperture focusing technique,” *IEEE Trans. Ultrason. Ferroelectr. Freq. Control*, vol. 61, no. 5, pp. 830–839, 2014.
[26] M. H. Bae and M.-K. Jeong, “A study of synthetic-aperture imaging with virtual source elements in B-mode ultrasound imaging systems,” *IEEE Trans. Ultrason. Ferroelectr. Freq. Control*, vol. 47, no. 6, pp. 1510–1519, 2000.
[27] S. Wu, H. Wu, H. Jin, K. Yang, and E. Wu, “Frequency-domain synthetic aperture focusing technique for immersion testing using focused transducer,” *J. Zhejiang Univ. (Engineering Sci.*, vol. 49, no. 1, pp. 110–115, 2015.
[28] M. Trelinski, “Inspection of CANDU Reactor Pressure Tubes Using Ultrasonics,” in *17th World Conference on Nondestructive Testing*, 2008, p. 8.
[29] T. Stepinski, “Technique in Ultrasonic Inspection of Coarse Grained Materials,” 2008.
[30] M. A. Fischler and R. C. Bolles, “Random Sample Consensus: A Paradigm for Model Fitting with,” *Commun. ACM*, vol. 24, pp. 381–395, 1981.